Electromagnetic Shielding of Resonant Frequency-Selective Surfaces in Presence of Dipole Sources

G. Lovat, R. Araneo, and S. Celozzi

Department of Astronautical, Electrical and Energetic Engineering
University of Rome "Sapienza", Via Eudossiana 18, 00184 Roma, Italy
giampiero.lovat, rodolfo.araneo, salvatore.celozzi@uniroma1.it

Abstract ─ The shielding problem consisting in the interaction between a dipole source and a Frequency-Selective Surface (FSS) is investigated. The Array Scanning Method (ASM) is adopted to take into account all the propagating and evanescent waves, which constitute the spectrum of the dipole and all the propagating and evanescent Floquet modes, which constitute the spectrum of the diffracted field by the FSS. The main differences with respect to the shielding of a conventional plane-wave source are pointed out, especially in terms of resonant frequencies, operating bandwidth and transmission levels.

Index Terms ─ Electromagnetic shielding, frequency selective surfaces and periodic structures.

I. INTRODUCTION

Frequency Selective Surfaces (FSSs) are periodic structures along two dimensions, often planar. They may consist of either metallic elements or apertures cut in a metallic plate, periodically arranged in a two-dimensional (2-D) array; multi-layer lattices are generally considered. The main characteristic of an FSS is its capability to be effectively reflecting Electromagnetic (EM) fields in a given frequency range and almost completely transparent out of this interval, showing filtering properties. FSSs are attractive for many applications and can act as polarizers, filters, subreflectors, RAMs, superstrates for antennas, shields; e.g., [1]. The FSS EM behavior and performance mainly depend on the geometry of the single element and on the spatial periods; moreover, in general, they are also quite sensitive to the characteristics of the incident wave (incident angles and polarization, if a conventional plane-wave excitation is used) [2]. In recent years, in addition to the study of artificial periodic screens with high-pass behaviors [3], [4], many efforts have been spent in order to design FSSs with miniaturized elements, polarization and angular stability and multiband operation [5]-[11].

However, very often, the incident field has been typically assumed as that of a uniform plane wave; only recently, the interaction between a finite source (such as an elemental dipole) and an infinite periodic structure has been addressed [4], [12]-[18] since the conventional Floquet theory cannot be applied directly and some alternatives must be explored.

The novelty of the present investigation with respect to published papers is resumed as follows:

i) First of all, as far as we know, this is the first time that the interaction between a dipole source and a resonant infinite periodic screen is considered. In previous works, the considered periodic screens were basically high-pass structures with no resonant properties.

ii) The resonant behavior of the considered structures allows us to investigate how classical figures of merit, such as level of transmission, resonant frequency, resonant bandwidth, etc., change when a finite dipole source is considered instead of a classical plane-wave excitation. In fact, when the dipole is close to the periodic screen the evanescent part of its spectrum can strongly interact with the periodic screen; thus, spoiling the classical plane-wave response

iii) Some peculiar behaviors are pointed out when vertical dipoles are considered. While far-

interacting horizontal dipoles mainly behave as suitably polarized plane waves, far-interacting vertical dipoles do not have the corresponding plane-wave counterparts; so the response of the periodic screens to such sources may be particularly interesting.

In this paper, the shielding properties of resonant FSSs in the presence of dipole sources in their proximity are studied. The frequency-selective behavior is first studied in the presence of a conventional plane-wave excitation in order to point out the standard and generally considered response; then more realistic electric and magnetic dipole sources characterized by different distances and orientations are analyzed.

II. DESCRIPTION OF THE PROBLEM

The EM configuration is reported in Fig. 1. It consists of an incident far or near field (which can be either that of a uniform plane wave or that of a near electric or magnetic-dipole source, respectively) impinging on an FSS periodic along the x and y directions with spatial periods p_x and p_y.
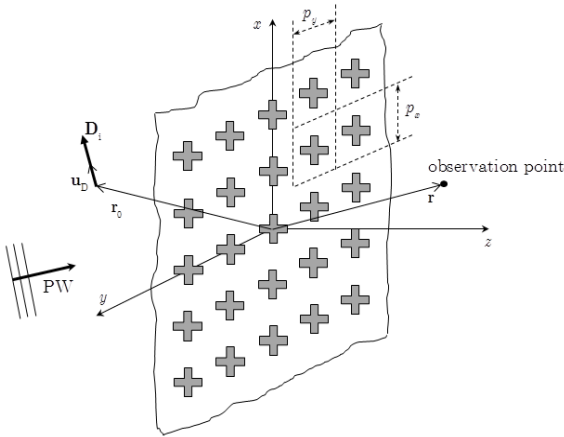
Fig. 1. Two-dimensional (2-D) periodic screen, excited either by a finite-dipole $\mathbf{D}_i$ or a plane-wave (PW) source.

The unit cell of the periodic FSS is constituted by Perfectly Conducting (PEC) elements or apertures cut in a PEC plane; a dielectric foam ($\varepsilon_r = 1$) is considered as host medium: different

dielectric hosts call for more sophisticated numerical acceleration techniques [19], [20] and for simplicity are not considered here, since the main features are not affected by this choice (except when unconventional substrates are used [21]).

A time-harmonic dependence $\mathrm{e}^{j\omega t}$ is assumed and suppressed throughout. The electric or magnetic shielding effectiveness (SE) is adopted as a performance parameter [22].

III. PLANE-WAVE EXCITATION

It is well known that in the presence of a plane-wave excitation (which is a particular type of Floquet-periodic source) the analysis can be simplified by restricting the computational domain (which in principle, is infinite) to a single unit cell by enforcing periodic boundary conditions and using a periodic Green's function [23]. The integral equation which describes the problem can next be obtained by enforcing the Electric-Field Integral Equation (EFIE); i.e., the null of the total tangential electric field on the PEC elements of the unit cell. The total electric field $\mathbf{E}_{\mathrm{tot}}$ is the sum of the incident plane-wave field $\mathbf{E}_{\mathrm{inc}}$ and the scattered field $\mathbf{E}_{\mathrm{sc}}$ given by:

$$\mathbf{E}_{\mathrm{sc}}\left(\mathbf{r}\right) = \int_S \underline{\mathbf{G}}_{\mathrm{p}}^{EJ}\left(\mathbf{r},\mathbf{r}'\right) \cdot \mathbf{J}_S\left(\mathbf{r}'\right) \mathrm{d}\mathbf{r}', \quad (1)$$

where $\underline{\mathbf{G}}_{\mathrm{p}}^{EJ}$ is the EJ-type dyadic periodic Green's function, $\mathbf{J}_S$ is the unknown current density induced over the surface S of the conductors within the unit cell and $\mathbf{r}$ and $\mathbf{r}'$ are the vectors from the origin to the source and observation points, respectively. The solution of the EFIE can be obtained by expanding the unknown $\mathbf{J}_S$ through suitable vector basis functions and applying a Galerkin testing procedure for the final discretization. From the knowledge of $\mathbf{J}_S$, the scattered field $\mathbf{E}_{\mathrm{sc}}$ (and thus, the total field $\mathbf{E}_{\mathrm{tot}}$) can finally be obtained.

In dealing with FSSs constituted by arrays of apertures cut in a PEC plane, the aforementioned integral equation can still be constructed with the electric current density $\mathbf{J}_S$ defined on the PEC surface of the unit cell. As an alternative, the

equivalence theorem may be applied by enforcing the continuity of the tangential magnetic field on the apertures of the unit cell surface A; thus, deriving an integral equation whose unknowns are equivalent magnetic currents $\mathbf{M}_A$. It is well-known that the kernel of the integral equation does not change; there is only a change in the unknown and in the incident field (the electric field in the former case, the magnetic field in the latter one).

Actually, to efficiently solve the derived integral equations by means of the MoM technique, it is numerically more convenient to recast them in a Mixed-Potential Integral Equation form (MPIE) [24], [25] by introducing the magnetic vector and electric scalar potentials $\mathbf{A}$ and V for electric sources $\mathbf{J}_S$ (and possibly the electric vector and magnetic scalar potentials $\mathbf{F}$ and W for magnetic sources $\mathbf{M}_A$), respectively; so that the convolution terms can be expressed as:

$$\mathbf{E}\ \mathbf{J} = \underline{\mathbf{G}}^{EJ} \otimes \mathbf{J} = -j\omega\mathbf{A} - \nabla V =$$
$$= -j\omega\underline{\mathbf{G}}^A \otimes \mathbf{J} + \frac{1}{j\omega}\nabla\ G^V \otimes \nabla \cdot \mathbf{J} \quad , \quad (2a)$$

$$\mathbf{H}\ \mathbf{J} = \underline{\mathbf{G}}^{HJ} \otimes \mathbf{J} = \frac{1}{\mu_0}\nabla \times \mathbf{A} =$$
$$= \frac{1}{\mu_0}\ \nabla \times \underline{\mathbf{G}}^A\ \otimes \mathbf{J} \quad , \quad (2b)$$

$$\mathbf{E}\ \mathbf{M} = \underline{\mathbf{G}}^{EM} \otimes \mathbf{M} = -\frac{1}{\varepsilon_0}\nabla \times \mathbf{F} =$$
$$= \frac{1}{\varepsilon_0}\ \nabla \times \underline{\mathbf{G}}^F\ \otimes \mathbf{M} \quad , \quad (2c)$$

$$\mathbf{H}\ \mathbf{M} = \underline{\mathbf{G}}^{HM} \otimes \mathbf{M} = -j\omega\mathbf{F} - \nabla W =$$
$$= -j\omega\underline{\mathbf{G}}^F \otimes \mathbf{M} + \frac{1}{j\omega}\nabla\ G^W \otimes \nabla \cdot \mathbf{M} \quad , (2d)$$

where the symbol $\otimes$ denotes the superposition integral, while $\underline{\mathbf{G}}^{A,F}$ and $G^{V,W}$ are the potential periodic 2-D Green's functions for electric or magnetic currents and charges, respectively; calculated by means of the Ewald method, the spectral and spatial representations of the periodic Green's function are combined to obtain a final expression in terms of a sum of two fast-decaying Gaussian convergent series [24]-[26]. The Ewald method has efficiently been applied also for 1-D

and 3-D periodic Green's functions [27], [28].

A standard MoM procedure is then considered; either the PEC parts or the apertures in the unit cell can be discretized through non-overlapping triangles and the unknown current densities ($\mathbf{J}_S$ or $\mathbf{M}_A$, respectively) can be expanded by a set of second-order subdomain basis functions, which provide a linear-normal/quadratic-tangent (LN/QT) representation of the vector quantities [29] and result more accurate and smoother than conventional RWG basis functions and first-order triangular patches (LL) [30]. All the singular terms present in the source integrals (proportional to $1 / |\mathbf{r} - \mathbf{r}'|$) can be extracted and integrated analytically [31], while the remaining (source and testing) integrals can be computed by means of standard Gaussian formulas [32].

IV. DIPOLE EXCITATION

The first step in the application of the ASM is the expression of the finite source as a superposition of infinite auxiliary Floquet periodic sources having the same periods of the original periodic structure. The well-known Floquet theory [23] can then be applied to each elemental Floquet-periodic problem (FPP, characterized by the values of the phase shifts q_x and q_y); thus, restricting the computational domain to a unit cell. Once the auxiliary FPPs are solved, the solution of the original problem is reconstructed by superposition through the ASM identity. In fact, for 2-D periodic configurations, the ASM exploits the following identity:

$$\delta\ \mathbf{r} - \mathbf{r}_0 = p_{xy}\int_{-\frac{\pi}{p_y}}^{+\frac{\pi}{p_y}}\int_{-\frac{\pi}{p_x}}^{+\frac{\pi}{p_x}}\sum_{m,n=-\infty}^{+\infty}\delta\ \mathbf{r} - \mathbf{r}_{mn}\ \cdot$$
$$\cdot e^{-j\ q_x m p_x + q_y n p_y}\ dq_x dq_y \quad , (3)$$

where

$$p_{xy} = \frac{p_x p_y}{2\pi^2} \quad , \quad (4)$$

$\delta\ \bullet$ is the Dirac delta generalized function, $\mathbf{r}_{mn} = \mathbf{r}_0 + \mathbf{p}_{mn}$, with $\mathbf{r}_0 = \mathbf{u}_x x_0 + \mathbf{u}_y y_0 + \mathbf{u}_z z_0$

and $\quad \mathbf{p}_{mn} = \mathbf{u}_x m p_x + \mathbf{u}_y n p_y$. Therefore, the single aperiodic dipole source $\mathbf{D}_i$ (where $\mathbf{D}_i$ can be either $\mathbf{J}_i$ or $\mathbf{M}_i$) directed along the unit vector $\mathbf{u}_D$ can be expressed as:

$$\mathbf{D}_i(\mathbf{r}) = D_0 \delta(\mathbf{r} - \mathbf{r}_0) \mathbf{u}_D =$$

$$= p_{xy} \int\limits_{-\frac{\pi}{p_y}}^{+\frac{\pi}{p_y}} \int\limits_{-\frac{\pi}{p_x}}^{+\frac{\pi}{p_x}} \mathbf{D}_i^{FP}(\mathbf{r}, q_x, q_y) \, dq_x dq_y , \quad (5)$$

with

$$\mathbf{D}_i^{FP}(\mathbf{r}, q_x, q_y) = D_0 \sum_{m,n=-\infty}^{+\infty} \delta(\mathbf{r} - \mathbf{r}_{mn}) \cdot$$
$$\cdot e^{-j(q_x m p_x + q_y n p_y)} \mathbf{u}_D \quad (6)$$

For each auxiliary source $\mathbf{D}_i^{FP}$ with phase shifts q_x and q_y, we have a single FPP; which can be solved as described in the previous section. With respect to the canonical problem involving a plane-wave excitation, the only difference is the incident field, which is now produced by a 2-D phased array of dipoles in free space. The total field due to each auxiliary source $\mathbf{D}_i^{FP}$ in the presence of the periodic structure is the sum of the incident field and of the field scattered by the periodic loading. The final step of the ASM procedure is the reconstruction of the total field produced by the dipole source through the superposition of the auxiliary total fields by means of the ASM identity (3).

Several details on the numerical implementation of the ASM for 2-D periodic structures can be found in [17]; features of the configurations considered in this work are presented in the next Section.

V. NUMERICAL RESULTS

Two different resonant FSSs are considered as case studies: a metallic Jerusalem-Cross (JC) and a Double-Loop (DL), shown in Figs. 2 (a) and 2 (b), respectively; with the relevant geometric parameters.

The structures have been designed in order to present the first resonant frequency at about 1.9 GHz.
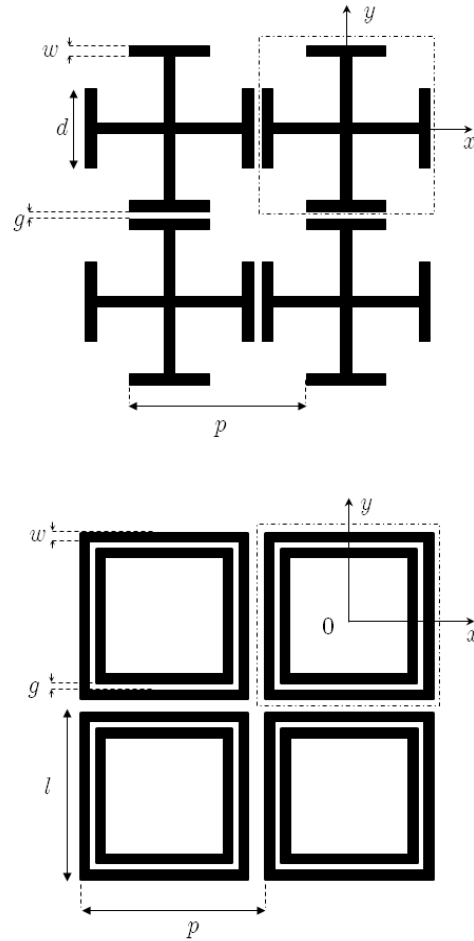
Fig. 2. Unit cells (dashed areas) of the two considered FSSs: Jerusalem-Cross (JC) and Double-Loop (DL). Parameters: p=3.44 cm, d=2.24 cm, w=0.16 cm and g=0.08 cm for the JC FSS and p=3.66 cm, l=3.33 cm, w=0.3 cm and g=0.3 cm for the DL FSS.

In all the reported results, both the dipole source and the observation point for SE evaluations have been located along the z axis (i.e., (x, y)=(0, 0), in the center of the unit cell); moreover, the observation point has also been placed in the far field at $z>50\,p$, for both the structures. In Fig. 3, we report the SE of the JC for incident (a) TE and (b) TM plane waves at θ=0, $\pi/6$, $\pi/3$ as a function of frequency f along the ϕ=0 plane. As it can be seen, for TE incidence, the resonant frequency of the periodic screen is quite stable at f_{res}=1.9 GHz; whereas, for TM incidence

is more sensitive to the incident angle, although it remains between 1.9 and 2 GHz.

(a)

(b)
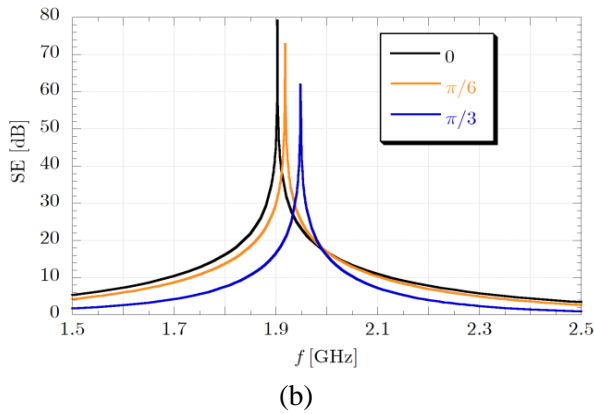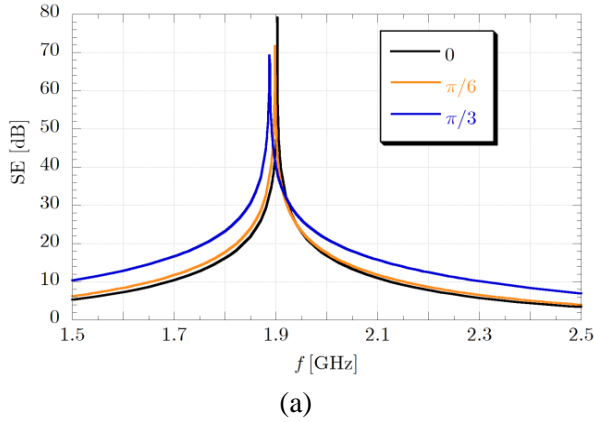
Fig. 3. SE of the metallic JC FSS in Fig. 2 as a function of frequency under: (a) TE and (b) TM plane-wave incidence for different incidence angles θ along the ϕ=0 plane.

It is then interesting to study how the SE changes by placing a dipole source at z_s closer and closer to the screen; thus, considering a real near-field source. This is illustrated in Fig. 4 at the operating frequency f_{res}=1.9 GHz. It can be seen that the SE for both horizontal and vertical dipoles of both electric and magnetic type can change by almost 20 dB with small variations of z_s (from 5 mm to 30 mm); whereas, for larger values of z_s, the horizontal dipole results converge to the normally-incident plane-wave SE (and the horizontal dipole; thus, gains the characteristics of a far-field source). This is consistent with the fact that a Horizontal Electric Dipole (HED) behaves in the far field as a TE plane wave, while a Horizontal Magnetic Dipole (HMD) as a TM plane wave; since source and observation points

lie along the z axis, the associated TE and TM plane waves behave as normally incident TEM plane waves.
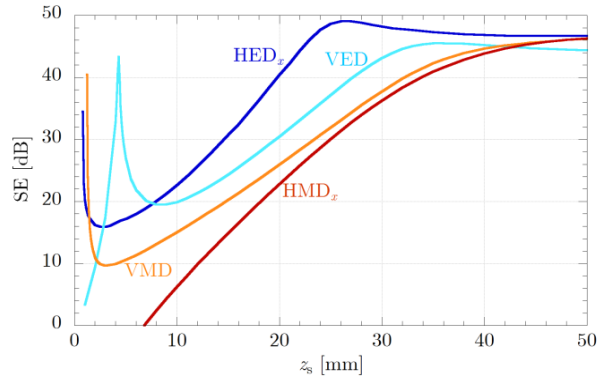
Fig. 4. SE of the JC FSS in Fig. 2 as a function of the dipole-screen distance z_s for different dipole types and orientations at the resonant frequency f_{res}=1.9 GHz for normal plane-wave incidence.

(a)

(b)
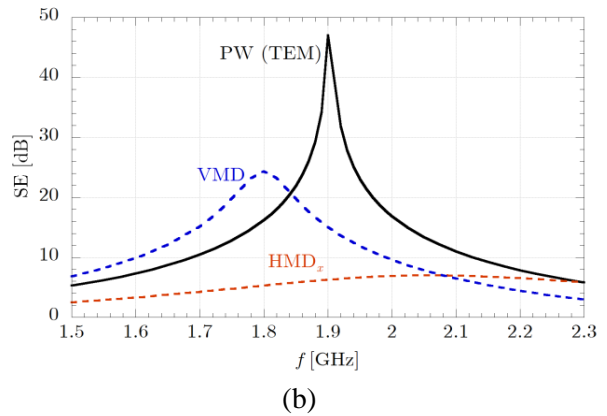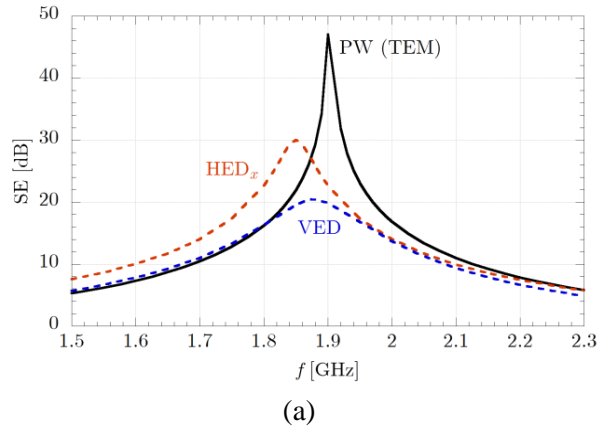
Fig. 5. SE of the JC FSS in Fig. 2 as a function of frequency for: (a) electric and (b) magnetic dipoles at the dipole-screen distance z_s=10 mm.

On the other hand, since vertical dipoles do not have a far field in their direction, it is not obvious that for large z_s their SE tends to a plane-wave SE; as it can be seen in Fig. 4, this actually occurs for the considered structure in the Vertical-Magnetic-Dipole (VMD) case, but not in the Vertical-Electric-Dipole (VED) case.

In general, for all the dipole sources the SE decreases by decreasing the dipole-screen distance z_s; however, for the VED, the SE presents a peak when the source is placed at a critical distance z_c very close to the screen at $z_c=4.3$ cm. Moreover, for $z_s=0$ the SE for the HED_x and the VMD tends to infinity, while for the VED and the HMD_x assumes a finite (low) value. Such a behavior can easily be understood taking into account that for $z_s=0$ the dipoles lie on the PEC part of the JC element, so that the HED x and VMD are short-circuited (and the relevant radiated field is zero), while the radiation of the VED and HMD_x are maximized.

In order to understand how the frequency-selective behavior varies in the presence of a finite source close to the screen, in Fig. 5 the SE is presented as a function of frequency using a conventional TEM plane-wave source and both an electric and a magnetic dipole (Figs. 5 (a) and 5 (b), respectively) with different orientations and with the dipole source placed at $z_s=10$ mm.

It can be observed that both the resonant frequency, the relevant bandwidth and the SE peak value change significantly, depending on the dipole type and orientation. In particular, assuming that the dominant part of the electric-dipole spectrum is constituted by TE plane waves and that of the magnetic-dipole spectrum by TM plane waves, it can be understood why the SE of a VMD and of a HMD presents stronger differences with respect to the SE of a normally incident plane wave. It is worth noting that in the HMD case the resonant behavior has completely disappeared.

In Fig. 6, the SE of the DL for incident (a) TE and (b) TM plane waves is reported at $\theta=0$, $\pi/6$, $\pi/3$ as a function of frequency along the $\phi=0$ plane. Two resonances are present and the shielding performance is quite similar for both polarizations; in particular, while the first resonance at $f_{res1} \simeq 2$ GHz is quite sensitive to the incident angle, the second resonance at $f_{res2}=2.32$

GHz is almost independent of the characteristics of the incident plane wave. Moreover, it is interesting to note that this type of screen is characterized by a frequency of total transmission $f_{TT}=2.25$ GHz (for which SE=0 db), which does not depend at all on the plane-wave properties.

(a)

(b)
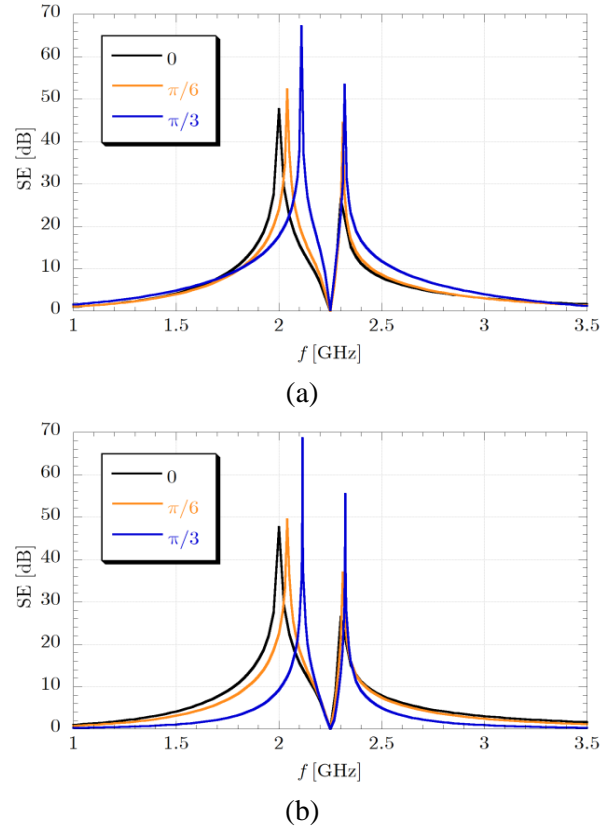
Fig. 6. SE of the DL FSS in Fig. 2 as a function of frequency under: (a) TE and (b) TM plane-wave incidence for different incidence angles θ along the $\phi=0$ plane.

When a dipole source is considered, the operation is similar to that already illustrated for the JC screen, except for the fact that now the SE for the HED_x and the VMD does not tend to infinity for source points approaching the screen plane, since in this case the source does not lie on a PEC part of the screen. This is shown in Fig. 7 at the operating frequency $f_{res1}=2$ GHz, where it can be seen that the SE monotonically decreases to low SE values by decreasing the dipole-screen distance z_s except for the VMD, which presents a SE peak at the critical distance $z_c=3.3$ cm and

maintains a considerably large SE value also for very small z_s (always larger than 20 db); the latter is consistent with the well-known fact that a closed loop strongly interacts with an orthogonal magnetic dipole.

Finally, also for the DL FSS, the SE is presented as a function of frequency using a conventional TEM plane-wave source and both an electric and a magnetic dipole placed at z_s=10 mm (Figs. 8 (a) and 8 (b), respectively) with different orientations. It can be observed, that also for this structure, both the resonant frequencies and the SE peak values strongly depend on the dipole type and orientation. In particular, the resonant characteristics almost completely disappear when a VED or an HMD source is considered. Finally, it is interesting to note that in the presence of dipole sources, the total transmission phenomenon is still present at the frequency f_{TT}=2.25 GHz.
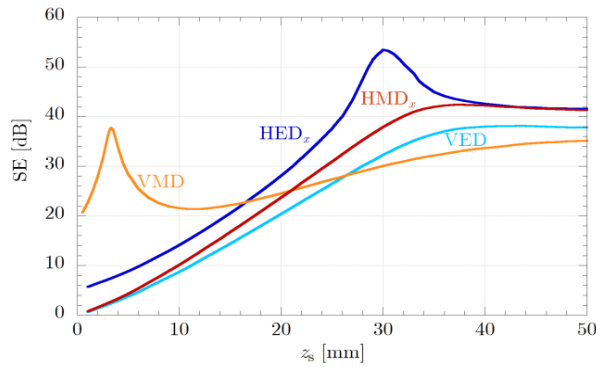
Fig. 7. SE of the DL FSS in Fig. 2 as a function of the dipole-screen distance z_s for different dipole types and orientations at the first resonant frequency f_{res1}=2 GHz for normal plane-wave incidence.

(a)

(b)
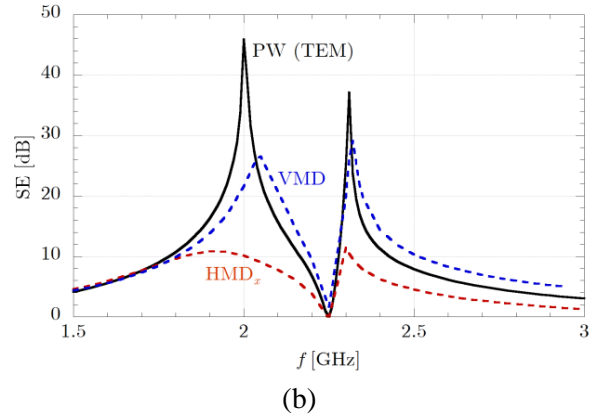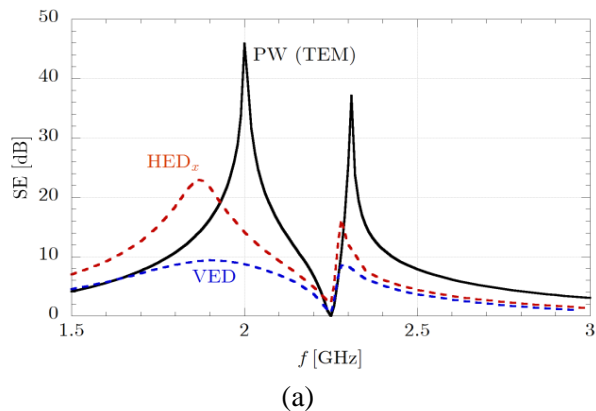
Fig. 8. SE of the DL FSS in Fig. 2 as a function of frequency for: (a) electric and (b) magnetic dipoles at the dipole-screen distance z_s=10 mm.

VI. CONCLUSION

The shielding characteristics of resonant frequency-selective periodic screens based on metallic FSSs in the presence of both plane-wave far-field and dipole near-field sources have been investigated. After an analysis based on a conventional plane-wave excitation, the interaction between the resonant screen and a finite near-field source placed in its proximity has been studied in detail, through a periodic MoM approach in conjunction with the Array Scanning Method. In particular, this analysis method allows for taking into account all the propagating and evanescent waves constituting the spectrum of the dipole source. It has been shown how the presence of finite sources can affect the resonant frequency and the relevant bandwidth of a frequency-selective screen; thus, calling for reliable numerical tools for the analysis and design and demonstrating how conclusions drawn on the basis of conventional PW excitation are not representative of the actual behavior of frequency selective shielding surfaces.

REFERENCES

[1] B. A. Munk, "Frequency selective surfaces: theory and design," *New York: Wiley*, 2000.
[2] A. S. Barlevy and Y. Rahmat-Samii, "On the electrical and numerical properties of high q resonances in frequency selective surfaces," *Progress In Electromagnetics Research*, vol. 22, pp. 1-27, 1999.
[3] G. Lovat, P. Burghignoli, and S. Celozzi, "Shielding properties of a wire-medium screen,"

IEEE Trans. Electromagn. Compat., vol. 50, no. 1, pp. 80-88, February 2008.

[4] R. Araneo, G. Lovat, and S. Celozzi, "Shielding effectiveness of periodic screens against finite high-impedance near-field sources," *IEEE Trans. Electromagn. Compat.*, vol. 53, no. 3, pp. 706-716, August 2011.

[5] J. van Tonder and U. Jakobus, "Infinite periodic boundary conditions in FEKO," *ACES Journal*, vol. 24, no. 6, pp. 584-591, 2009.

[6] B. Lin, S. Du, H. Zhang, and X. Ye, "Design and simulation of frequency-selective radome together with a monopole antenna," *ACES Journal*, vol. 25, no. 7, pp. 620-625, 2010.

[7] A. Yakovlev, C. Simovski, S. Tretyakov, and G. Hanson, "Accurate and rapid analysis of high impedance surfaces: plane-wave and surface-wave analytical models," *In ACES Conference Paper-Modeling Techniques for Periodic Structures and Metamaterial Applications-I*, 2010.

[8] J. Romeu and Y. Rahmat-Samii, "Fractal FSS: a novel dual-band frequency selective surface," *IEEE Trans. Antennas Propag.*, vol. 48, no. 7, pp. 1097-1105, July 2000.

[9] S. Barbagallo, A. Monorchio, and G. Manara, "Small periodicity FSS screens with enhanced bandwidth performance," *Electronics Letters*, vol. 42, pp. 382-384, 2006.

[10] K. Sarabandi and N. Behdad, "A frequency selective surface with miniaturized elements," *IEEE Trans. Antennas Propag.*, vol. 55, no. 5, pp. 1239-1245, May 2007.

[11] B. Sanz-Izquierdo, E. A. Parker, J. B. Roberson, and J. C. Batchelor, "Singly and dual polarized convoluted frequency selective structures," *IEEE Trans. Antennas Propag.*, vol. 58, no. 3, pp. 690-696, March 2010.

[12] A. M. Attiya, "Dyadic green's function of an elementary point source above a periodically-defected-grounded dielectric slab," *Progress In Electromagnetics Research B*, vol. 4, pp. 127-145, 2008.

[13] G. Lovat, "Near-field shielding effectiveness of 1-D periodic planar screens with 2-D near-field sources," *IEEE Trans. Electromagn. Compat.*, vol. 51, no. 3, pp. 708-719, August 2009.

[14] G. Lovat and P. Burghignoli, "Propagation and field excitation in metalstrip grating waveguides: homogeneous model and full-wave analysis," *IEEE Antennas Wireless Propag. Lett.*, vol. 8, pp. 708-711, 2009.

[15] S. Paulotto, G. Lovat, P. Baccarelli, and P. Burghignoli, "Green's function calculation for a line source exciting a 2-D periodic printed structure," *IEEE Microw. Wireless Compon. Lett.*, vol. 20, no. 4, pp. 181-183, April 2010.

[16] S. Paulotto, P. Baccarelli, P. Burghignoli, G. Lovat, G. Hanson, and A. Yakovlev, "Homogenized green's functions for an aperiodic line source over planar densely periodic artificial impedance surfaces," *IEEE Trans. Microw. Theory Tech.*, vol. 58, no. 7, pp. 1807-1817, July 2010.

[17] G. Lovat, R. Araneo, and S. Celozzi, "Dipole excitation of periodic metallic structures," *IEEE Trans. Antennas Propag.*, vol. 59, no. 6, pp. 2178-2189, June 2011.

[18] G. Lovat, R. Araneo, and S. Celozzi, "Planar and bulk resonant periodic screens against plane-wave and electric-dipole excitations," *In Proc. IEEE Electromagn. Compat. Symp.*, pp. 623-628, August 5-10, 2012.

[19] G. Valerio, P. Baccarelli, S. Paulotto, F. Frezza, and A. Galli, "Regularization of mixed-potential layered media greens functions for efficient interpolation procedures in planar periodic structures," *IEEE Trans. Antennas Propag.*, vol. 57, no. 1, pp. 122-134, January 2009.

[20] H. Bahadori, H. Alaeian, and R. Faraji-Dana, "Computation of periodic green's functions in layered media using complex images technique," *Progress In Electromagnetics Research*, vol. 112, pp. 225-240, 2011.

[21] G. Lovat, P. Burghignoli, and S. Celozzi, "A tunable ferroelectric antenna for fixed-frequency scanning applications," *IEEE Antennas Wireless Propag. Lett.*, vol. 5, pp. 353-356, 2006.

[22] R. Araneo, G. Lovat, S. Celozzi, and M. D'Amore, "Shielding performance of nanostructured transparent thin films loading apertures of metallic enclosures excited by dipole sources," *In Proc. IEEE Electromagn. Compat. Symp.*, pp. 214-219, August 14-19, 2011.

[23] A. F. Peterson, S. L. Ray, and R. Mittra, "Computational methods for electromagnetics," *Piscataway, NJ: IEEE Press*, 1998.

[24] I. Stevanovic, P. Crespo-Valerio, K. Blagovi´c, F. Bongard, and J. R. Mosig, "Integral-equation analysis of 3-D metallic objects arranged in 2-D lattices using the ewald transformation," *IEEE Trans. Microw. Theory Tech.*, vol. 54, no. 10, pp. 3688-3697, October 2006.

[25] J. Su, X. W. Xu, M. He, and K. Zhang, "Integral equation analysis of frequency selective surfaces using ewald transformation and lattice symmetry," *Progress In Electromagnetics Research*, vol. 121, pp. 249-269, 2011.

[26] S. Oroskar, D. R. Jackson, and D. R. Wilton, "Efficient computation of the 2D periodic green's function using the ewald method," *J. Comput. Phys.*, vol. 219, pp. 899-911, September 2006.

[27] F. Capolino, D. Wilton, and W. Johnson, "Efficient computation of the 3D green's function for the

helmholtz operator for a linear array of point sources using the ewald method," *J. Comput. Phys.*, vol. 223, no. 1, pp. 250-261, 2007.

[28] G. Lovat, P. Burghignoli, and R.Araneo, "Efficient evaluation of the three-dimensional periodic green's function through the ewald method," *IEEE Trans. Microw. Theory Tech.*, vol. 56, no. 9, pp. 2069-2075, 2008.

[29] K. R. Aberegg, A. Taguchi, and A. F. Peterson, "Application of higher-order vector basis functions to surface integral equation formulations," *Radio Sci.*, vol. 31, pp. 1207-1213, September 1996.

[30] R. Araneo and G. Lovat, "Analysis of the shielding effectiveness of metallic enclosures excited by internal sources through an efficient method of moment approach," *ACES Journal*, vol. 25, no. 7, pp. 600-611, July 2010.

[31] R. D. Graglia, "On the numerical integration of the linear shape functions times the 3-D green's function or its gradient on a plane triangle," *IEEE Trans. Antennas Propag.*, vol. 41, no. 10, pp. 1448-1455, October 1993.

[32] D. A. Dunavant, "High degree efficient symmetrical gaussian quadrature rules for the triangle," *Intern. J. Num. Meth. Engin.*, vol. 21, pp. 1129-1148, June 1985.

Giampiero Lovat received his Laurea degree (*cum laude*) in Electronic Engineering and his Ph.D. degree in Applied Electromagnetics from Sapienza University of Rome, Rome, in 2001 and 2005. From January 2004 to July 2004 he was a Visiting Scholar at the University of Houston, Houston, TX. In 2005, he joined the Department of Electrical Engineering, Sapienza University of Rome, where he is currently an Assistant Professor. His current research interests include electrodynamics of graphene and carbon nanotubes, energy harvesting by means of piezoelectric nanowires, leaky waves, periodic structures, artificial materials and electromagnetic shielding.

Rodolfo Araneo received his M.S. (cum laude) and Ph.D. degrees in Electrical Engineering from the University of Rome "La Sapienza", Rome, in 1999 and 2002. His research activity is mainly in the field of EMC and includes numerical and analytical techniques for modeling high-speed printed circuit boards, shielding, and transmission line analysis. He has authored more than 110 papers in international journals and conference proceedings.

Salvatore Celozzi is Full Professor of Electrical Engineering with the Department of Astronautical, Electrical and Energetic Engineering at the University of Rome "La Sapienza." Celozzi has published more than 120 papers in international journals or conference proceedings, mainly in the fields of electromagnetic shielding and transmission lines. He served as Associate Editor of the IEEE Electromagnetic Compatibility (1995-2000) and authored a book on Electromagnetic Shielding for Wiley in 2008. His current research interests include transmission lines, electromagnetic compatibility, meta and piezo-materials and numerical methods in electromagnetics.